ResearchGate

See discussions, stats, and author profiles for this publication at: https://www.researchgate.net/publication/281621200

Ab Initio Assessment of the Structural and Optoelectronic Properties of Organic–ZnO Nanoclusters

ARTICLE *in* THE JOURNAL OF PHYSICAL CHEMISTRY A · SEPTEMBER 2015

Impact Factor: 2.69 · DOI: 10.1021/acs.jpca.5b04109

READS

27

2 AUTHORS, INCLUDING:

Pushpendra Kumar

Indian Institute of Technology Mandi

3 PUBLICATIONS **4** CITATIONS

SEE PROFILE

Available from: Pushpendra Kumar

Retrieved on: 25 January 2016

THE JOURNAL OF PHYSICAL CHEMISTRY A

Article

pubs.acs.org/JPCA

Ab Initio Assessment of the Structural and Optoelectronic Properties of Organic–ZnO Nanoclusters

Pushpendra Kumar and Suman Kalyan Pal*

School of Basic Sciences and Advanced Materials Research Center, Indian Institute of Technology Mandi, Kamand, Mandi 175005, Himachal Pradesh, India

Supporting Information

ABSTRACT: Structural, electronic, and optical properties of a new coumarin dye, zinc oxide (ZnO) nanoclusters of varying sizes, and their complexes have been investigated using density functional theory (DFT). The band gap of oxide nanoclusters varies with size validating quantum confinement effect in small particles. Energy level diagrams of dye, ZnO nanoclusters, and redox electrolyte are in favor of efficient electron injection from dye to nanocluster and regeneration of the ionized dye. The adsorption of the organic dye to nanocluster is tested for anchoring through three different functional groups (cyano, carbonyl, and hydroxyl) of the dye. We have compared simulated absorption spectra of the dye, nanoclusters, and dye functionalized nanoclusters and discussed the matching with the solar irradiance spectrum. A strong new band appeared in the low energy side of the absorption spectra for dye adsorbed nanoclusters. Frontier molecular orbital calculations reveal that the first absorption band of dye–ZnO complexes is charge transfer (CT) in character. Excitation of this band leads to direct electron transfer to the conduction band (CB) of the nanocluster, making dye–ZnO complexes suitable for type II DSSCs as well.

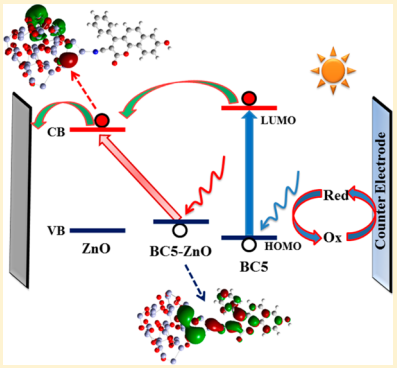

1. INTRODUCTION

One of the recent challenges is energy harvesting from clean and renewable sources. Dye-sensitized solar cells (DSSCs) have attracted much attention as an alternative, inexpensive, and environmentally friendly means for converting sunlight into electricity since Gratzel and co-workers developed it in 1991.[1,2] In DSSCs, solar radiation is absorbed by dye molecules attached to the wide band gap semiconductor, typically TiO_2, and injects photoelectron into the conduction band (CB) of the semiconductor.[3] The electron then goes to the adjacent conducting oxide electrode. Oxidized dye is regenerated by accepting an electron from the other electrode via electrolyte (e.g., I_3^-/I^-), making that electrode positive and developing a photovoltage.

The performance of DSSCs largely depends on dye sensitizers. Ru–polypyridine complexes are widely used dyes, which exhibit efficiencies (η) higher than 12%.[4] Over the past few years there has been a growing interest in organic dyes as substitutes of noble metal complexes due to many advantages, such as diversity of molecular structures, high molar extinction coefficient, simple synthesis, as well as low cost and environmental issues. A number of merocyanine,[5] indoline,[6] coumarin,[7,8] polyene,[9] hemicyanine,[10,11] triphenylamine,[12−14] phenothiazine,[15] fluorene[16−18] and tetrahydroquinoline[19] based-organic dyes have been used in DSSC and efficiency as high as 9% could be achieved.

TiO_2 is the most widely used n-type semiconductor in the DSSC devices. However, other metal oxides like SnO_2, ZnO, Nb_2O_5 and WO_3 are also being devoted to a significant deal of research.[20−22] Particularly, ZnO and SnO_2 have gathered more interest because of their over 2 orders of magnitude higher electron mobility than TiO_2 in bulk phases.[20,23−25] Nevertheless, the efficiency of the ZnO-based DSSCs ($\eta \approx 8\%$) is quite unsatisfactory with comparison to TiO_2 devices ($\eta \approx 12\%$).[4] One possible reason for this lower efficiency could be that at the edge of conduction band, ZnO displays much smaller density of states as compared to TiO_2, which makes electron injection into the conduction band from photoexcited dye less favorable.[26] Moreover, with the reduction of the size in nanocluster, conduction band experiences a significant upward shift due to the quantum confinement effects and probability of electron injection into conduction band edge from photoexcited dye decreases. However, the exact reasons underlying the relatively poor performance of ZnO are still a matter of debate.

In DSSCs, electron transfer from the photoexcited dye to the semiconductor nanomaterials is the most important process. DSSCs are categorized into type I and type II depending on the nature of electron transfer. In type I, excited electron moves from the LUMO of the dye to the CB of semiconductor, whereas in type II, electron from the HOMO of the dye jumps directly to the CB via charge transfer (CT) transition.[27] Recently, efforts have been made to establish a molecular understanding of photoinduced electron transfer in dye anchored

Received: April 29, 2015
Revised: September 3, 2015

ACS Publications © XXXX American Chemical Society

DOI: 10.1021/acs.jpca.5b04109
J. Phys. Chem. A XXXX, XXX, XXX−XXX

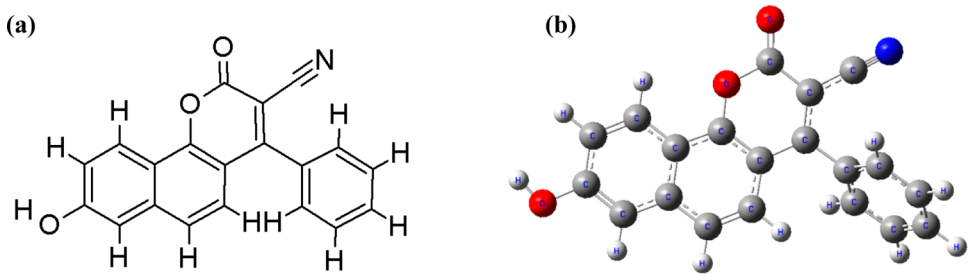

Figure 1. Molecular structure (a) with its ground state optimized geometry (b) of the BC5 dye.

nanoparticles using theoretical calculations.[3,28−34] These studies considered both metal complexes and organic dyes with carboxylate binding groups. However, computational investigation of the ground and excited state properties of nanoparticle functionalized by a dye via anchoring group other than carboxylate is still lagging.

In this work, our efforts are directed toward ab initio calculations of the structure and DSSC related optoelectronic properties of coumarin dye, 8-hydroxy-2-oxo-4-phenyl-2*H*-benzo-[*h*]chromene-3-carbonitrile (BC5)[35] (Figure 1), $(ZnO)_n$ clusters, and BC5−$(ZnO)_n$ complexes for n = 3, 6, 9, 12, 21, and 34. The dye is newly synthesized, and its ground and excited state properties have not been explored yet. The strong interaction of the BC5 with ZnO nanoclusters is favorable because of its push−pull character (donor−π−acceptor) due to the presence of an electron donating hydroxyl group and withdrawing cyanide group. Here, for the first time we report strong adsorption of dye onto ZnO nanocluster via the cyano group. Our DFT calculations reveal that energy level alignments are favorable for efficient electron transfer from the BC5 to ZnO nanoclusters. Simulated UV−vis spectra of the BC5−ZnO system shift toward red compared to only dye, suggesting more matching with the solar spectrum. Moreover, we successfully demonstrated that BC5−$(ZnO)_n$ complexes are suitable for type II DSSCs.

2. COMPUTATIONAL METHODS

All ground and excited state calculations were performed using density functional theory (DFT)[36−38] with the help of the hybrid generalized gradient approximation (GGA) Becke−Lee−Yang−Parr three-parameter (B3LYP) exchange-correlation functional[39] in the Gaussian 09 software suite.[40] Singlet to singlet transitions were calculated with the time-dependent density functional theory (TD-DFT)[41] following ground state geometry optimization. Normal mode analysis (i.e., frequency calculation) has been done for all the systems to find the true local minimum by avoiding saddle points. In all the cases, absence of imaginary frequencies confirms the successful optimization of the molecular structure with minimum energy. GaussSum 2.2 software[42] was exploited to simulate molecular orbitals (MOs), UV−vis absorption spectra, and density of states (DOS).

UV−vis absorption spectra of BC5 molecule was modeled using different basis sets such as STO-3G, 3-21G, 6-31G, 6-31G (d), 6-311G, 6-311G (d,p), and LANL2DZ. Both polarizable continuum model (PCM)[43,44]with the integral equation formalism (IEF) and conductor-like polarizable continuum model (CPCM)[45] were used to model the effect of the solvent tetrahydrofuran (THF) on the electronic and optical properties. The reason behind the choice of the solvent is to compare the simulated absorption spectra of the dye with reported experimental spectra in THF.[35] Moreover, THF was previously used as a solvent to study similar systems.[46,47] We modeled different size zinc oxide clusters $(ZnO)_n$, for n = 3, 6, 9, 12, 21, and 34. Although, wurtzite structure is the most stable polymorph of the ZnO under the ambient condition,[48] the actual crystal structure of ZnO nanoclusters is still a matter of debate. Wang et al.[49] reported hollow cagelike structure of $(ZnO)_{34}$ cluster, whereas others[50,51] found sodalite structure as the most stable structure. Here, ZnO clusters were initially constructed based on wurtzite bulk structure, as suggested by previous reports.[28,52] The LANL2DZ core pseudopotentials and associated double-ξ quality valence basis functions were used for heavy Zn atoms in ZnO clusters and BC5 functionalized ZnO clusters. The adsorption energy of the dye for the BC5−ZnO complex was estimated using the relation

$$E_{ads} = E(\text{BC5−ZnO complex}) - E(\text{ZnO cluster}) - E(\text{BC5}) \quad (1)$$

3. RESULTS AND DISCUSSION

3.1. BC5 Dye. Proper matching of the absorption spectra of the dye with the solar irradiation spectra increases both light absorption and charge generation efficiencies and thereby enhances the overall performance of DSSCs. We simulated UV−vis absorption spectra of the BC5 in both vacuum and solvent using TD-DFT method. TD-DFT calculations typically provide the information on transition energies, molar extinction coefficient, oscillator strengths, and molecular orbital compositions corresponding to each transition. The simulated UV−vis absorption spectra of BC5 for some particular level of basis sets (STO-3G, 3-21G, 6-31G (d) and LanL2DZ) in vacuum as well as in THF are shown in Figure 2a and Figure 2b, respectively. However, major electronic transitions corresponding to all basis sets are presented in (Table S1 (vacuum) and Tables S2 and S3 (THF), Supporting Information). Simulated absorption spectra clearly indicate a systematic red shift of the low energy band position while moving from smaller to larger basis sets in vacuum as well as in solvent. This is because of the fact that molecule gets more degrees of freedom for larger basis set in comparison with smaller one.

A comparison of absorption spectra in vacuum and THF for a particular basis set (6-31G (d)) is shown in Figure S1a (Supporting Information). The low energy absorption band undergoes a significant red shift (∼20 nm) along with an increment in molar extinction coefficient in the solvent. The observed solvatochromic shift is due to the dielectric screening of the solvent dipoles in polar environment. As in the polar environment, the dipole moments of the dye in the ground and excited states are different, resulting different stabilization of the ground and excited states and hence a change in the energy gap

DOI: 10.1021/acs.jpca.5b04109
J. Phys. Chem. A XXXX, XXX, XXX−XXX

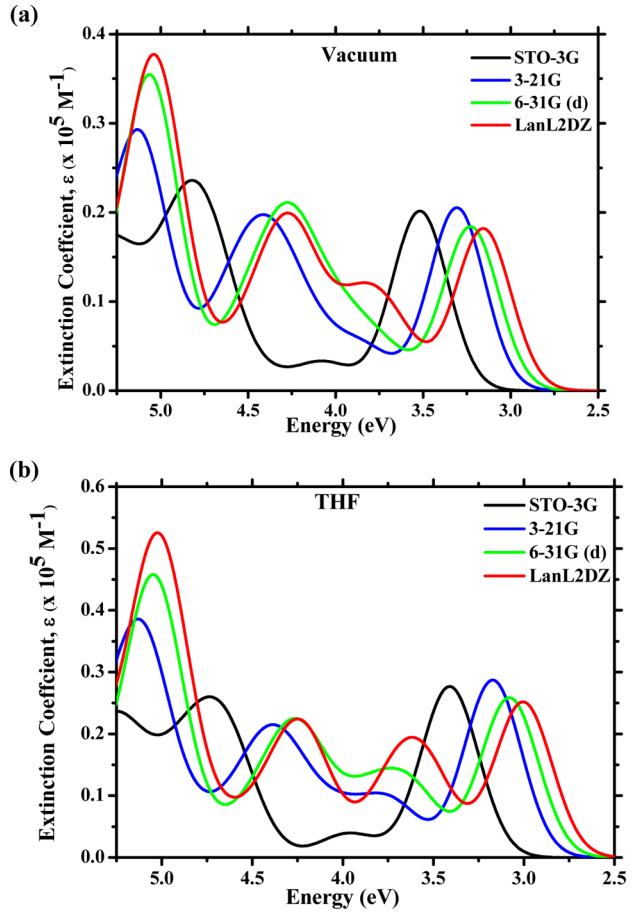

Figure 2. Simulated UV−vis absorption spectra of the BC5 calculated by TD-DFT at different levels of basis sets in (a) vacuum and (b) THF.

between them. In order to investigate the effect of various salvation models on transition energies, we calculated vertical transitions of the BC5 molecule in THF using both polarizable continuum model (PCM) with the integral equation formalism (IEF) and conductor-like polarizable continuum model (CPCM). These results are presented in the Tables S2 and S3 (Supporting Information). Simulated absorption spectra for both the models (Figure S1b, Supporting Information) perfectly overlap with each other, indicating that any one of those salvation models is sufficient for the modeling of BC5 in the THF environment.

Detailed information about electronic transitions and corresponding oscillator strengths with orbital contributions in THF is presented in Table S4 (Supporting Information). The simulated absorption spectra of the BC5 in THF with major electronic transitions is displayed in Figure S2 (Supporting Information). The experimental absorption spectra of BC5 in THF show peaks at 3.10 eV (400 nm), 3.55 eV (350 nm), and 4.21 eV (295 nm)[35] that are in good agreement with the calculated transitions. These results suggest that medium basis set (like 6-31G(d)) may be sufficient to model the BC5 molecule and the expensive calculations involving bigger basis sets can be avoided. It is clear from the simulated data (Supporting Information Table S4) that main contributions for peaks at 3.08 eV (403 nm), 3.61 eV (344 nm), and 4.22 eV (294 nm) are originating from HOMO (highest occupied molecular orbital) → LUMO (lowest unoccupied molecular orbital), HOMO − 1 → LUMO and HOMO → LUMO + 1, respectively. Whereas both HOMO − 1 → LUMO + 1 and HOMO → LUMO + 2 contribute equally for 5.03 eV (247 nm) peak. The isodensity surfaces of the key molecular orbitals for BC5 depict the π and π^* character of HOMO and LUMO, respectively (Figure S2). Therefore, the lowest energy transition (3.08 eV) is mainly $\pi \rightarrow \pi^*$ in nature.

3.2. Zinc Oxide Nanoclusters. The study of the properties of ZnO clusters is quite imperative in order to get insight into the dye−nanocluster interaction. In this context, the modeling of ZnO clusters of different sizes (number of atoms are 6, 12, 18, 24, 42, and 68) has been carried out. Ground state optimized structures of all clusters are shown in Figure 3. Modeled structure of $(ZnO)_{34}$ before the optimization is shown in Supporting Information Figure S3, which is slightly distorted after geometry optimization because of the minimization of the surface stresses.[53]

A quantity that really influences the charge generation and hence the performance of DSSCs is the position of the CB edge. The analysis of the partial density of states (pDOS) of nanoclusters provides the information about the contribution of atomic orbitals in CB and VB (valence band), respectively. Figure 4a shows the pDOS spectra for bigger size clusters calculated by DFT/B3LYP/LanL2DZ level of theory in vacuum (pDOS spectra of other clusters are shown in Figure S4a). It is apparent from the pDOS spectra that VB is mainly contributed by oxygen 2p atomic orbitals, while CB is associated with zinc 4s orbital. The computed energies of the VB and CB edges and band gap for all the clusters, including dye are shown in Table S5 (Supporting Information). The VB edge is significantly affected by the variation in the size of the nanocluster, and it increases with the increase in cluster size, whereas there is no particular trend in the variation of CB edge energy with the increase in cluster size; it increases up to the cluster $(ZnO)_{12}$, then decreases for $(ZnO)_{21}$ and further enhances slightly for $(ZnO)_{34}$. The variation in CB energy is comparatively less than the VB energy. However, the band gap was found to be decreased systematically with increasing number of atoms in the cluster. A regular decrement in the band gap was observed with increasing cluster size, which could be attributed to the quantum confinement effect in nanoclusters.

The optical properties of $(ZnO)_n$ (n = 3, 6, 9, 12, 21, and 34) clusters were investigated by calculating vertical transitions in vacuum using TD-DFT/B3LYP/LANL2DZ level of theory. Total of 20 singlet states were calculated. Energies, oscillator strengths, and orbital contributions for these transitions are presented in Table S6 (Supporting Information). Figure S4b (Supporting Information) and Figure 4b depict the absorption spectra of isolated $(ZnO)_n$ (n = 3, 6, 9, 12, 21, and 34) clusters. The absorption spectra of ZnO clusters show molecular characteristic with several peaks at different energy positions. There is a clear red shift of the absorption spectra as one move from small to large size cluster, due to the weaker confinement of an exciton in larger clusters.[28]

3.3. Alignment of Energy Levels and Electron Transfer. Proper alignment of the energy levels of dye and nanocluster is very important for efficient generation of charges in DSSCs. Position of HOMO and LUMO of BC5 with CB and VB edge for all simulated ZnO clusters and bulk ZnO[54] is shown in Figure 5. The CB edge of clusters and LUMO of the BC5 are represented by red solid bars, while the VB edge and HOMO are represented by blue solid bars. The LUMO of the BC5 lies well above the CB edge of the ZnO clusters favoring efficient electron injection from photoexcited BC5 to oxide

DOI: 10.1021/acs.jpca.5b04109
J. Phys. Chem. A XXXX, XXX, XXX−XXX

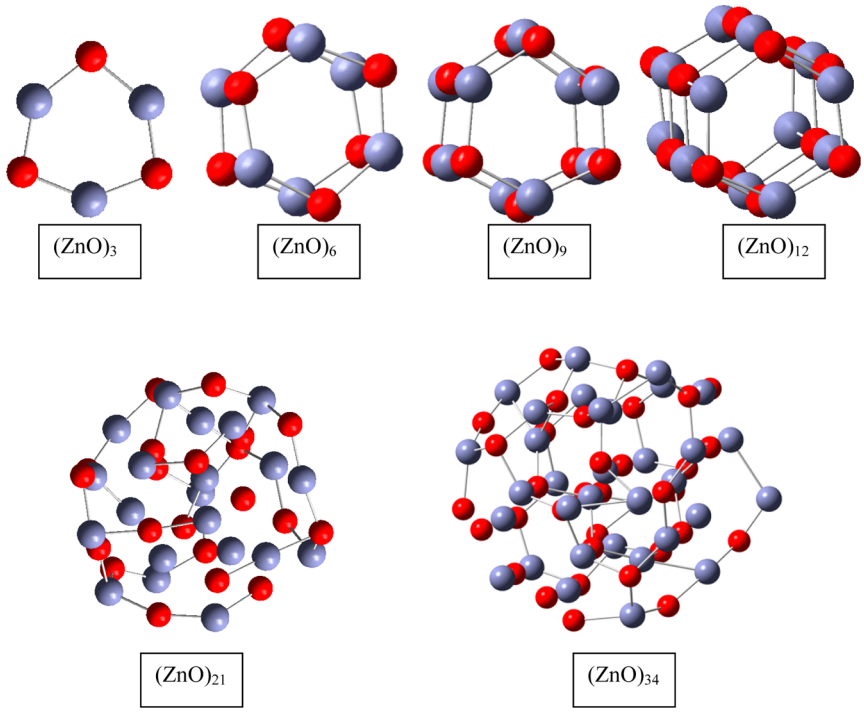

Figure 3. Optimized structures of ZnO clusters performed at the DFT/B3LYP/LanL2DZ level of theory in vacuum. Color code: blue for zinc and red for oxygen atoms.

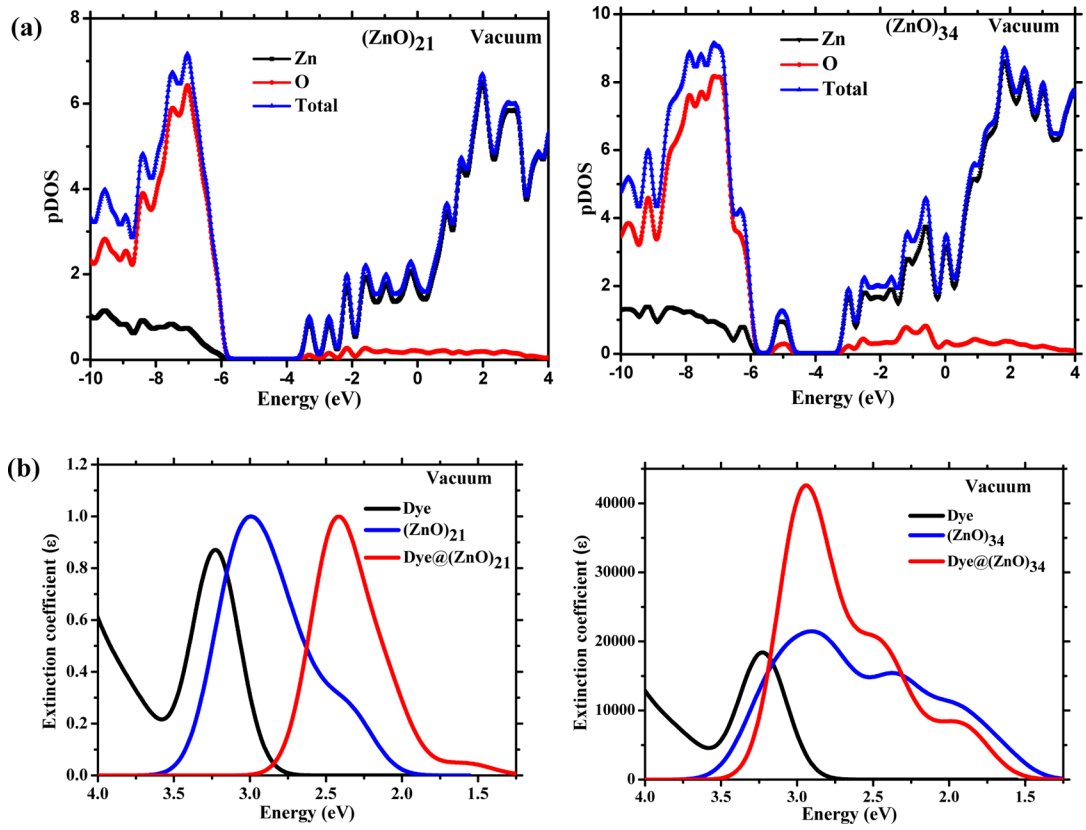

Figure 4. (a) Total and partial density of states (pDOS) of $(ZnO)_n$ clusters for n = 21 and 34. (b) Simulated absorption spectra of isolated dye (black), $(ZnO)_n$ clusters (blue), and BC5−$(ZnO)_n$ complexes (red) with cyano anchoring.

nanoclusters. The energy difference between LUMO of the BC5 and CB edge of the ZnO cluster provides driving force for the electron injection.[55] The calculated values of the driving force (in vacuum) for ZnO clusters $(ZnO)_3$, $(ZnO)_6$, $(ZnO)_9$ $(ZnO)_{12}$, $(ZnO)_{21}$, and $(ZnO)_{34}$ are 0.63, 0.58, 0.43, 0.38, 0.82, and 0.54 eV, respectively.

It has been reported that the rate of electron injection increases for higher driving force, i.e., when the dye excited

DOI: 10.1021/acs.jpca.5b04109
J. Phys. Chem. A XXXX, XXX, XXX−XXX

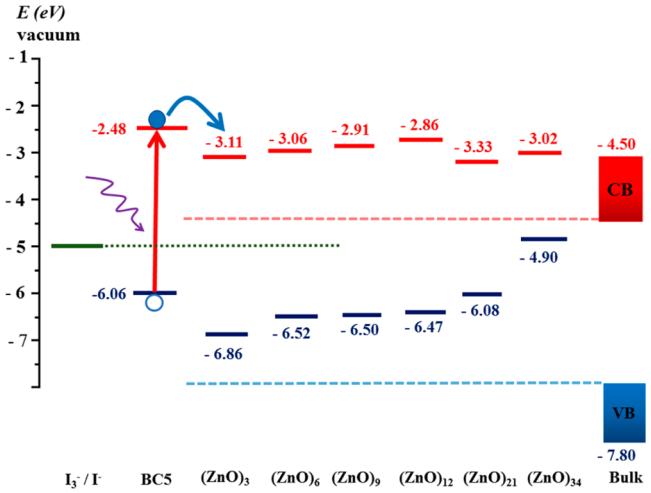

Figure 5. Energy level diagram displays the ground state (blue) and excited state (red) energies of the BC5 in vacuum with respect to the VB and CB edge of the $(ZnO)_n$ cluster for n = 3, 6, 9, 12, 21, and 34, bulk ZnO and redox energy of triiodide/iodide. The representation of dotted lines makes an easier examination of the energy level alignment for the eyes.

state lies well above the edge of the conduction band.[56] A larger value of the driving force may cause a more rapid electron injection and hence improves the overall efficiency of the device.[57] The speed of electron injection might be increased because of large driving force.[53] But it does not always increase short circuit current density and device efficiency.[53] There are instances where device efficiency varies inversely with the driving force. The experimentally measured power conversion efficiency for a number of coumarin dyes increases with decreasing driving force.[58−60] Therefore, it is not wise to correlate the overall device efficiency directly with the driving force for electron injection because the efficiency depends on many more factors.[53] Moreover, electron injection rate increases with the increase of driving force; if electron transfer occurs in the "Marcus normal region", in the "Marcus inverted region", rate and driving force follow an inverse relation.[61,62]

The regeneration of the dye could also be realized efficiently, as the HOMO level of the BC5 lies sufficiently below the redox level of the electrolyte triiodide/iodide (I_3^-/I^-). These observation suggest that BC5 and ZnO nanoclusters are good candidates for type I DSSCs. Nonetheless, it has been shown that the energy level alignment can substantially change after the dye absorption on nanocluster surface,[63] but that may not affect the electron injection. Pratik et al.[29] observed that the efficient electron injection is possible from the adsorbed dye to the TiO_2 nanocluster. We also have demonstrated electron transfer from BC5 dye to ZnO nanocluster in the complex (see section 3.5).

The isodensity surfaces of the HOMO and LUMO levels of the BC5 (Figure S2) have been evaluated extensively with the aim to explore the possibility of electron transfer from the dye to nanoclusters. In the HOMO and LUMO, the electron density is localized on the main coumarin unit as well as on the three functional groups cyano (−C≡N), carbonyl (C═O), and hydroxyl (−OH), respectively. The presence of electron density on the HOMO of these functional groups suggests that charge transfer can occur in the ground state and the BC5 can form ground state charge transfer (CT) complex with ZnO nanoclusters via bonding with any one of these functional groups. However, since the electron density is relatively more (5% and 9% than carbonyl and hydroxyl groups, respectively) on the cyano group, the adsorption of the BC5 onto ZnO cluster via CT interaction through cyano group is more favorable. The electron density sufficiently reduced on the carbonyl and the hydroxyl groups in the LUMO in comparison to the HOMO due to the electron donating nature of these groups, whereas a small increment is observed in the cyano group due to its electron accepting nature. These results indicate that the excited state electron injection probability will be more in the case of dye adsorption to the nanocluster via the cyano group.

3.4. Adsorption of Dye on ZnO Nanoclusters. With the knowledge of isolated dye and nanoclusters, we continued to investigate the electronic properties of BC5 adsorbed ZnO clusters of varying size. The type of bonding and electronic coupling between the excited state of dye and the unoccupied states of semiconductor has a direct effect on the overall efficiency of DSSCs.[1,64,65] BC5 can be anchored to the surface of a nanocluster via any one or two of the three functional groups. The electronic properties of the composite system can significantly be affected by the mode of anchoring of the BC5 to the nanocluster surface. Therefore, identification of the most favorable mode of adsorption is important. Here, we tested adsorption of the BC5 with all the anchoring groups to the ZnO clusters (Supporting Information Figure S5). We investigated both monodentate (where BC5 was bound to a single Zn atom of the cluster via any one of the three functional groups) and bridging (anchoring with two Zn atoms of the cluster through both cyano and carbonyl groups) attachments (Table 1). The initial length of the anchoring bond (N/O−metal) was fixed at 2.20 Å, but after optimization of all modes of attachments a slight decrement in the bond length was observed that could be due to the good electron affinity of ZnO.

The adsorption energy (E_{ads}) of BC5−ZnO systems was calculated from the total energy of isolated BC5, ZnO clusters, and their complex using eq 1. Table 1 summarizes the calculated bond lengths and adsorption energies for BC5−ZnO composite systems for all modes of attachment of BC5 with nanoclusters in vacuum. Negative values of E_{ads} ensure that all complexes studied are stable. The significant values of the adsorption energies indicate that the BC5 molecules are strongly bound to the surface of the ZnO clusters.

It is clear from the Table 1 that the adsorption energy is found to be low for hydroxyl group in the case of all ZnO nanoclusters, which makes it unfavorable compared to the other anchoring groups. In spite of the close proximity of cyano and carbonyl groups, the adsorption energy of bridging attachment is less than monodentate anchoring through each of these groups. For smaller clusters (up to 24 atoms), adsorption energies are comparable for binding through both cyano and carbonyl groups. However, in the case of bigger clusters (number of atoms being 42 and 68), the adsorption energies are much higher for anchoring via cyano group than carbonyl unit. The highest absolute value of the adsorption energy and the smallest Zn−N bond length indicate that the monodentate attachment of the BC5 via cyno group is the most stable geometry with the strong interaction between dye and nanocluster. Recently, Hedrick et al.[28] reported an adsorption energy of −1.07 eV for the bridging attachment of a Ru(II)−polybipyridine complex with $(ZnO)_{33}$ cluster via the carboxylate group. It should be noted that our calculated adsorption energy (−1.36 eV) for the binding of the dye with a ZnO cluster of

DOI: 10.1021/acs.jpca.5b04109
J. Phys. Chem. A XXXX, XXX, XXX−XXX

Table 1. Computed Bond Lengths and Adsorption Energies (E_{ads}) of BC5−ZnO Nanoclusters in Vacuum

system	anchoring group	mode of attachment[a] initial	final	bond length (Å)	E_{ads} (eV)
BC5−$(ZnO)_3$	−C≡N	md	md	2.09 (CN−Zn)	−1.28
	C═O	md	md	2.07 (O−Zn)	−1.29
	C═O/−C≡N	br	md	2.09 (CN−Zn)	−1.28
	−OH	md	md	2.08 (OH−Zn)	−1.14
BC5−$(ZnO)_6$	−C≡N	md	md	2.09 (CN−Zn)	−1.17
	C═O	md	md	2.08 (O−Zn)	−1.17
	C═O/−C≡N	br	br	2.12 (O−Zn)	−1.06
				2.33 (CN−Zn)	
	−OH	md	md	2.09 (OH−Zn)	−1.02
BC5−$(ZnO)_9$	−C≡N	md	md	2.10 (CN−Zn)	−1.12
	C═O	md	md	2.09 (O−Zn)	−1.09
	C═O/−C≡N	br	br	2.16 (O−Zn)	−1.08
				2.24 (CN−Zn)	
	−OH	md	md	2.10 (OH−Zn)	−0.97
BC5−$(ZnO)_{12}$	−C≡N	md	md	2.11 (CN−Zn)	−1.08
	C═O	md	md	2.09 (O−Zn)	−1.12
	C═O/−C≡N	br	br	2.12 (O−Zn)	−1.06
				2.30 (CN−Zn)	
	−OH	md	md	2.10 (OH−Zn)	−1.00
BC5−$(ZnO)_{21}$	−C≡N	md	md	2.11 (CN−Zn)	−2.52
	C═O	md	md	2.10 (O−Zn)	−2.49
	C═O/−C≡N	br	br	2.08 (O−Zn)	−1.88
				2.19 (CN−Zn)	
	−OH	md	md	2.09 (OH−Zn)	−2.32
BC5−$(ZnO)_{34}$	−C≡N	md	md	2.10 (Zn−N)	−1.36
	C═O	md	br	2.18 (Zn−O)	−1.14
				2.20 (Zn−N)	
	C═O/−C≡N	br	br	2.18 (Zn−O)	−1.14
				2.20 (Zn−N)	
	−OH	md	md	2.20 (Zn−O)	−0.58

[a]md = monodentate; br = bridging.

similar size via cyano group is found to be higher than that reported for carboxylate attachment.

3.5. Optical Properties of Adsorbed BC5 on ZnO Nanoclusters. The spectral properties of isolated BC5 and $(ZnO)_n$ clusters are already discussed in sections 3.1 and 3.2, respectively. In order to examine in detail the optical properties of BC5−$(ZnO)_n$ complex (for n = 3, 6, 9, 12, 21, and 34) anchored through cyano group, vertical transitions were calculated using TD-DFT. The absorption spectra of BC5−$(ZnO)_n$ for n = 21 and 34, in vacuum are presented in Figure 4b (the rest is in the Supporting Information. Figure S4b). A new band in the visible region of the solar spectra appears in the absorption spectra of dye adsorbed ZnO clusters. This band position for BC5−$(ZnO)_n$ with n = 3, 6, 9, and 12 is at ∼2.20 eV, but for BC5−$(ZnO)_{21}$ and BC5−$(ZnO)_{34}$ the positions are at ∼1.55 and ∼1.85 eV, respectively. The uncertainty in band position for large cluster is due to unstabilization of the surface states.

To elucidate the solvent effect on the electronic properties of BC5−ZnO complex, DFT and TD-DFT calculations were performed in THF using PCM model with integral equation formalism (IEF). It should be noted that Saba et al.[66] reported strong interaction between THF and ZnO cluster, which makes our choice of implicit solvent model questionable. In order to verify the possibility of THF adhesion on the ZnO clusters, we have estimated the binding energy between THF and $(ZnO)_{34}$ nanocluster following a similar procedure that was used for BC5−ZnO complexes. The adsorption energy (−0.71 eV) turns out to be almost half of the BC5−$(ZnO)_{34}$ complex (−1.36 eV). The observed stronger interaction of $(ZnO)_{34}$ with BC5 than THF suggests that our solvent choice is legitimate. A total of 50 singlet−singlet electronic transitions were calculated to cover up to UV region of the spectra. Figure 6 depicts the simulated absorption spectra of BC5, $(ZnO)_{34}$ cluster, and BC5−$(ZnO)_{34}$ complex in THF. The absorption spectra of BC5−$(ZnO)_{34}$ complex in THF exhibits a new band in the lower energy region similar to BC5−$(ZnO)_n$ complexes (for n = 3, 6, 9, 12, 21, and 34) in vacuum. Unlike the absorption spectra in vacuum (Supporting Information Figure S4), the new band in the solvent is more distinct and pronounced. Similar solvent effect was observed for dye−ZnO complexes of other smaller nanoclusters. This intense band in the visible part of the solar spectrum could enhance the light absorption and thereby increase the efficiency of DSSCs, provided the charges are formed as a result of absorption of light in this region. In order to know the possibility of photoinduced charge generation in BC5−$(ZnO)_n$ complexes, frontier molecular orbitals corresponding to relevant transitions were calculated.

The lowest energy band of BC5−$(ZnO)_{34}$ has highest oscillator strength and arises because of the HOMO → LUMO electronic transition (Supporting Information Table S7). The frontier molecular orbital pictures corresponding to HOMO and LUMO are displayed in Figure 6. In the HOMO of BC5−$(ZnO)_{34}$ complex, the electron density is localized over both

DOI: 10.1021/acs.jpca.5b04109
J. Phys. Chem. A XXXX, XXX, XXX−XXX

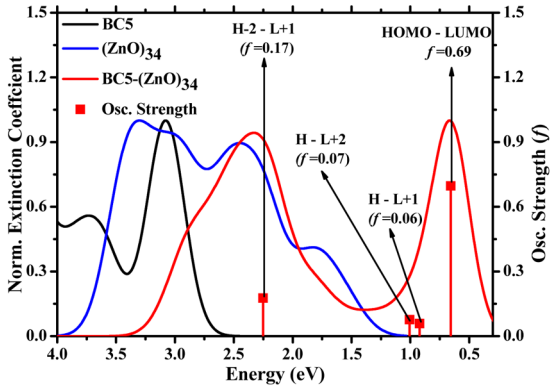

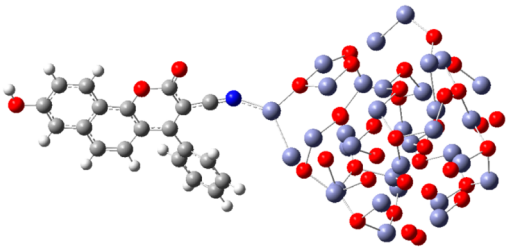

Optimised geometry of BC5-$(ZnO)_{34}$ attached with cyano group

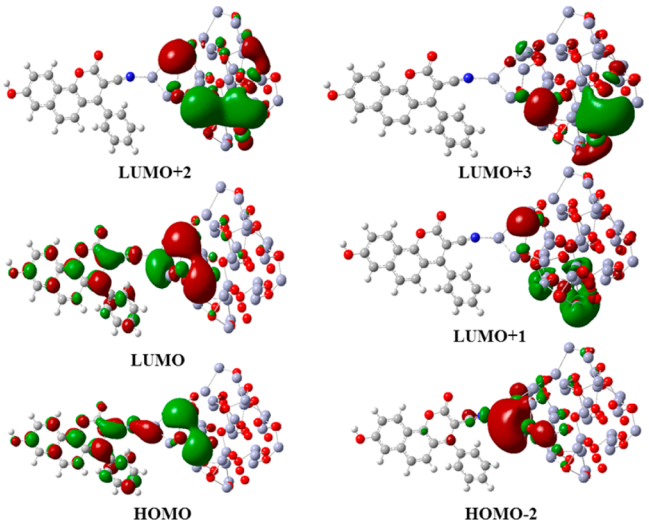

Figure 6. Simulated absorption spectra of BC5 (black), $(ZnO)_{34}$ cluster (blue), and their composite BC5−$(ZnO)_{34}$ (red) calculated by TD-DFT/B3LYP/LANL2DZ in THF. The oscillator strength (f) for BC5−$(ZnO)_{34}$ complex was represented by a vertical line at corresponding excited state energy. Optimized geometry of BC5−$(ZnO)_{34}$ complex with cyano group attachment and isodensity surface of frontier molecular orbitals corresponding to electronic transitions having high oscillator strength.

the BC5 and $(ZnO)_{34}$ cluster, indicating the formation of ground state charge transfer (CT) complex between BC5 and ZnO cluster. However, in the LUMO, electron density shifts more toward $(ZnO)_{34}$ cluster from the BC5. Frontier orbitals (HOMO − 2, LUMO + 1, LUMO + 2, and LUMO + 3) corresponding to higher energy electronic transitions were also calculated and shown in Figure 6. It is apparent from the orbital pictures that HOMO − 2 is mostly distributed over $(ZnO)_{34}$, whereas electron density is fully localized on ZnO clusters for LUMO + 1, LUMO + 2, and LUMO + 3. The other two major electronic transitions corresponding to the low energy absorption band are associated with HOMO → LUMO + 1 and HOMO → LUMO + 2. These observations suggest that the low energy absorption band of the complex is CT in nature and excitation of this band leads to charge transfer directly to ZnO cluster. Therefore, BC5−$(ZnO)_{34}$ complex with cyano anchoring is expected to be suitable for type II DSSCs. It should also be noted that not only CT excitation but higher energy excitations, e.g., HOMO − 2 → LUMO + 1, may also lead to the efficient electron transfer from BC5 to ZnO nanocluster.

4. CONCLUSION

We successfully simulated structures and optoelectronic properties of a coumarin dye, different size ZnO clusters, and dye−ZnO nanocluster complexes using first-principles calculations. The simulated UV−vis spectra of the isolated dye BC5 is basis set dependent but solvation method independent. The band gap of ZnO clusters decreases with the increase in particle size, revealing quantum confinement in nanoclusters. The position of the CB of nanoclusters is well below the LUMO of the dye in the energy level diagram, making electron injection from the excited BC5 to ZnO clusters favorable. The attachment of BC5 to the nanocluster surface by monodentate anchoring through the cyano group is the strongest one. A new intense CT band appears in the red side of the absorption spectra for the BC5−ZnO complex and the excitation of which resulted into the injection of electron directly to the CB of ZnO. Thus, these results suggest that the dye BC5 and ZnO nanoclusters are suitable for both type I and type II DSSCs.

■ ASSOCIATED CONTENT

Supporting Information

The Supporting Information is available free of charge on the ACS Publications website at DOI: 10.1021/acs.jpca.5b04109.

Details of the major vertical transitions of the BC5 dye in both vacuum and solvent (for solvation models IEFPCM and CPCM), unoptimized structure of the largest ZnO cluster, computed HOMO, LUMO, and band gap energies of isolated BC5 dye and $(ZnO)_n$ nanoclusters, major vertical transitions of $(ZnO)_n$ clusters, DOS and pDOS and simulated spectra of $(ZnO)_n$ and BC5−$(ZnO)_n$ complex for n = 3, 6, 9, and 12, various modes of the anchoring of the BC5 with $(ZnO)_n$ (n = 3, 6, 9, 12, 21, and 34) clusters, and major vertical transitions of the BC5−$(ZnO)_{34}$ complex in THF. (PDF)

■ AUTHOR INFORMATION

Corresponding Author

*Phone: +91 1905 267040. Fax: +91 1905 237924. E-mail: suman@iitmandi.ac.in.

Notes

The authors declare no competing financial interest.

■ ACKNOWLEDGMENTS

The authors sincerely acknowledge the financial support from Indian Institute of Technology (IIT) Mandi in the form of seed grant (Grant IITM/SG/SUG/004) and fellowship. Thanks are extended to Dr. S. Ghosh and S. Kumar, IIT Mandi, for the idea of a novel dye. We are also thankful to Dr. U. Sarkar, Assam University, for his initial help in the modeling of the ZnO cluster.

DOI: 10.1021/acs.jpca.5b04109
J. Phys. Chem. A XXXX, XXX, XXX−XXX

REFERENCES

(1) Gratzel, M. Photoelectrochemical Cells. *Nature (London, U. K.)* **2001**, *414*, 338−344.

(2) O'Regan, B.; Gratzel, M. A Low-Cost, High-Efficiency Solar Cell Based on Dye-Sensitized Colloidal Tio2 Films. *Nature* **1991**, *353*, 737−740.

(3) Pastore, M.; Fantacci, S.; De Angelis, F. Modeling Excited States and Alignment of Energy Levels in Dye-Sensitized Solar Cells: Successes, Failures, and Challenges. *J. Phys. Chem. C* **2013**, *117*, 3685−3700.

(4) Yella, A.; Lee, H.-W.; Tsao, H. N.; Yi, C.; Chandiran, A. K.; Nazeeruddin, M. K.; Diau, E. W.-G.; Yeh, C.-Y.; Zakeeruddin, S. M.; Graetzel, M. Porphyrin-Sensitized Solar Cells with Cobalt (Ii/Iii)-Based Redox Electrolyte Exceed 12% Efficiency. *Science (Washington, DC, U. S.)* **2011**, *334*, 629−634.

(5) Sayama, K.; Hara, K.; Sugihara, H.; Arakawa, H.; Mori, N.; Satsuki, M.; Suga, S.; Tsukagoshi, S.; Abe, Y. Photosensitization of a Porous Tio_2 Electrode with Merocyanine Dyes Containing a Carboxyl Group and a Long Alkyl Chain. *Chem. Commun. (Cambridge, U. K.)* **2000**, 1173−1174.

(6) Horiuchi, T.; Miura, H.; Sumioka, K.; Uchida, S. High Efficiency of Dye-Sensitized Solar Cells Based on Metal-Free Indoline Dyes. *J. Am. Chem. Soc.* **2004**, *126*, 12218−12219.

(7) Hara, K.; Sayama, K.; Arakawa, H.; Ohga, Y.; Shinpo, A.; Suga, S. A Coumarin-Derivative Dye Sensitized Nanocrystalline TiO_2 Solar Cell Having a High Solar-Energy Conversion Efficiency up to 5.6%. *Chem. Commun. (Cambridge, U. K.)* **2001**, 569−570.

(8) Hara, K.; Wang, Z.-S.; Sato, T.; Furube, A.; Katoh, R.; Sugihara, H.; Dan-oh, Y.; Kasada, C.; Shinpo, A.; Suga, S. Oligothiophene-Containing Coumarin Dyes for Efficient Dye-Sensitized Solar Cells. *J. Phys. Chem. B* **2005**, *109*, 15476−15482.

(9) Hara, K.; et al. Novel Conjugated Organic Dyes for Efficient Dye-Sensitized Solar Cells. *Adv. Funct. Mater.* **2005**, *15*, 246−252.

(10) Wang, Z.-S.; Li, F.-Y.; Huang, C.-H. Highly Efficient Sensitization of Nanocrystalline Tio_2 Films with Styryl Benzothiazolium Propylsulfonate. *Chem. Commun. (Cambridge, U. K.)* **2000**, 2063−2064.

(11) Yao, Q.-H.; Meng, F.-S.; Li, F.-Y.; Tian, H.; Huang, C.-H. Photoelectric Conversion Properties of Four Novel Carboxylated Hemicyanine Dyes on TiO_2 Electrode. *J. Mater. Chem.* **2003**, *13*, 1048−1053.

(12) Velusamy, M.; Thomas, K. R. J.; Lin, J. T.; Hsu, Y.-C.; Ho, K.-C. Organic Dyes Incorporating Low-Band-Gap Chromophores for Dye-Sensitized Solar Cells. *Org. Lett.* **2005**, *7*, 1899−1902.

(13) Kitamura, T.; Ikeda, M.; Shigaki, K.; Inoue, T.; Anderson, N. A.; Ai, X.; Lian, T.; Yanagida, S. Phenyl-Conjugated Oligoene Sensitizers for TiO_2 Solar Cells. *Chem. Mater.* **2004**, *16*, 1806−1812.

(14) Hagberg, D. P.; Edvinsson, T.; Marinado, T.; Boschloo, G.; Hagfeldt, A.; Sun, L. A Novel Organic Chromophore for Dye-Sensitized Nanostructured Solar Cells. *Chem. Commun. (Cambridge, U. K.)* **2006**, 2245−2247.

(15) Tian, H.; Yang, X.; Chen, R.; Pan, Y.; Li, L.; Hagfeldt, A.; Sun, L. Phenothiazine Derivatives for Efficient Organic Dye-Sensitized Solar Cells. *Chem. Commun. (Cambridge, U. K.)* **2007**, 3741−3743.

(16) Kim, S.; Lee, J. K.; Kang, S. O.; Ko, J.; Yum, J. H.; Fantacci, S.; De Angelis, F.; Di Censo, D.; Nazeeruddin, M. K.; Graetzel, M. Molecular Engineering of Organic Sensitizers for Solar Cell Applications. *J. Am. Chem. Soc.* **2006**, *128*, 16701−16707.

(17) Kim, D.; Lee, J. K.; Kang, S. O.; Ko, J. Molecular Engineering of Organic Dyes Containing N-Aryl Carbazole Moiety for Solar Cell. *Tetrahedron* **2007**, *63*, 1913−1922.

(18) Choi, H.; Lee, J. K.; Song, K.; Kang, S. O.; Ko, J. Novel Organic Dyes Containing Bis-Dimethylfluorenyl Amino Benzo[B] Thiophene for Highly Efficient Dye-Sensitized Solar Cell. *Tetrahedron* **2007**, *63*, 3115−3121.

(19) Chen, R.; Yang, X.; Tian, H.; Sun, L. Tetrahydroquinoline Dyes with Different Spacers for Organic Dye-Sensitized Solar Cells. *J. Photochem. Photobiol., A* **2007**, *189*, 295−300.

(20) Tiwana, P.; Docampo, P.; Johnston, M. B.; Snaith, H. J.; Herz, L. M. Electron Mobility and Injection Dynamics in Mesoporous Zno, Sno_2, and Tio_2 Films Used in Dye-Sensitized Solar Cells. *ACS Nano* **2011**, *5*, 5158−5166.

(21) Katoh, R.; Furube, A.; Yoshihara, T.; Hara, K.; Fujihashi, G.; Takano, S.; Murata, S.; Arakawa, H.; Tachiya, M. Efficiencies of Electron Injection from Excited N3 Dye into Nanocrystalline Semiconductor (ZrO_2, TiO_2, ZnO, Nb_2O_5, SnO_2, In_2O_3) Films. *J. Phys. Chem. B* **2004**, *108*, 4818−4822.

(22) Fessenden, R. W.; Kamat, P. V. Rate Constants for Charge Injection from Excited Sensitizer into SnO_2, ZnO, and TiO_2 Semiconductor Nanocrystallites. *J. Phys. Chem.* **1995**, *99*, 12902−6.

(23) Look, D. C.; Reynolds, D. C.; Sizelove, J. R.; Jones, R. L.; Litton, C. W.; Cantwell, G.; Harsch, W. C. Electrical Properties of Bulk Zno. *Solid State Commun.* **1998**, *105*, 399−401.

(24) Jarzebski, Z. M.; Marton, J. P. Physical Properties of Tin(IV) Oxide Materials. II. Electrical Properties. *J. Electrochem. Soc.* **1976**, *123*, 299C−310C.

(25) Shanthi, E.; Dutta, V.; Banerjee, A.; Chopra, K. L. Electrical and Optical Properties of Undoped and Antimony-Doped Tin Oxide Films. *J. Appl. Phys.* **1980**, *51*, 6243−51.

(26) Szarko, J. M.; Neubauer, A.; Bartelt, A.; Socaciu-Siebert, L.; Birkner, F.; Schwarzburg, K.; Hannappel, T.; Eichberger, R. The Ultrafast Temporal and Spectral Characterization of Electron Injection from Perylene Derivatives into ZnO and TiO_2 Colloidal Films. *J. Phys. Chem. C* **2008**, *112*, 10542−10552.

(27) Tae, E. L.; Lee, S. H.; Lee, J. K.; Yoo, S. S.; Kang, E. J.; Yoon, K. B. A Strategy to Increase the Efficiency of the Dye-Sensitized TiO_2 Solar Cells Operated by Photoexcitation of Dye-to-TiO_2 Charge-Transfer Bands. *J. Phys. Chem. B* **2005**, *109*, 22513−22522.

(28) Hedrick, M. M.; Mayo, M. L.; Badaeva, E.; Kilina, S. First-Principles Studies of the Ground- and Excited-State Properties of Quantum Dots Functionalized by Ru(Ii)-Polybipyridine. *J. Phys. Chem. C* **2013**, *117*, 18216−18224.

(29) Pratik, S. M.; Datta, A. Computational Design of Concomitant Type-I and Type-II Porphyrin Sensitized Solar Cells. *Phys. Chem. Chem. Phys.* **2013**, *15*, 18471−18481.

(30) Labat, F.; Ciofini, I.; Hratchian, H. P.; Frisch, M. J.; Raghavachari, K.; Adamo, C. Insights into Working Principles of Ruthenium Polypyridyl Dye-Sensitized Solar Cells from First Principles Modeling. *J. Phys. Chem. C* **2011**, *115*, 4297−4306.

(31) Anselmi, C.; Mosconi, E.; Pastore, M.; Ronca, E.; De Angelis, F. Adsorption of Organic Dyes on TiO_2 Surfaces in Dye-Sensitized Solar Cells: Interplay of Theory and Experiment. *Phys. Chem. Chem. Phys.* **2012**, *14*, 15963−15974.

(32) Le Bahers, T.; Pauporte, T.; Laine, P. P.; Labat, F.; Adamo, C.; Ciofini, I. Modeling Dye-Sensitized Solar Cells: From Theory to Experiment. *J. Phys. Chem. Lett.* **2013**, *4*, 1044−1050.

(33) Pastore, M.; De Angelis, F. Intermolecular Interactions in Dye-Sensitized Solar Cells: A Computational Modeling Perspective. *J. Phys. Chem. Lett.* **2013**, *4*, 956−974.

(34) Maggio, E.; Martsinovich, N.; Troisi, A. Using Orbital Symmetry to Minimize Charge Recombination in Dye-Sensitized Solar Cells. *Angew. Chem., Int. Ed.* **2013**, *52*, 973−975.

(35) Kumar, S.; Singh, P.; Srivastava, R.; Koner, R. R.; Pramanik, A.; Mathew, J.; Sinha, S.; Rawat, M.; Anand, R. S.; Ghosh, S. Engineering Fused Coumarin Dyes: A Molecular Level Understanding of Aggregation Quenching and Tuning Electroluminescence Via Alkyl Chain Substitution. *J. Mater. Chem. C* **2014**, *2*, 6637−6647.

(36) Hohenberg, P.; Kohn, W. Inhomogeneous Electron Gas. *Phys. Rev.* **1964**, *136*, B864−B871.

(37) Kohn, W.; Sham, L. J. Self-Consistent Equations Including Exchange and Correlation Effects. *Phys. Rev.* **1965**, *140*, A1133−A1138.

(38) Parr, R. G.; Yang, W. *Density-Functional Theory of Atoms and Molecules*; Oxford University Press: New York, NY, USA, 1989.

(39) Lee, C.; Yang, W.; Parr, R. G. Development of the Colle-Salvetti Correlation-Energy Formula into a Functional of the Electron Density. *Phys. Rev. B: Condens. Matter Mater. Phys.* **1988**, *37*, 785−789.

DOI: 10.1021/acs.jpca.5b04109
J. Phys. Chem. A XXXX, XXX, XXX−XXX

(40) Frisch, M. J.; et al. *Gaussian 09*, revision D.01; Gaussian Inc.: Wallingford, CT, 2009.
(41) Runge, E.; Gross, E. K. U. Density-Functional Theory for Time-Dependent Systems. *Phys. Rev. Lett.* **1984**, *52*, 997−1000.
(42) O'Boyle, N. M.; Tenderholt, A. L.; Langner, K. M. cclib: A Library for Package-Independent Computational Chemistry Algorithms. *J. Comput. Chem.* **2008**, *29*, 839−845.
(43) Barone, V.; Cossi, M. Quantum Calculation of Molecular Energies and Energy Gradients in Solution by a Conductor Solvent Model. *J. Phys. Chem. A* **1998**, *102*, 1995−2001.
(44) Tomasi, J.; Mennucci, B.; Cammi, R. Quantum Mechanical Continuum Solvation Models. *Chem. Rev. (Washington, DC, U. S.)* **2005**, *105*, 2999−3093.
(45) Hariharan, P. C.; Pople, J. A. The Influence of Polarization Functions on Molecular Orbital Hydrogenation Energies. *Theoretica chimica acta* **1973**, *28*, 213−222.
(46) Briseno, A. L.; Holcombe, T. W.; Boukai, A. I.; Garnett, E. C.; Shelton, S. W.; Frechet, J. J. M.; Yang, P. Oligo- and Polythiophene/Zno Hybrid Nanowire Solar Cells. *Nano Lett.* **2010**, *10*, 334−340.
(47) Das, K.; Jain, B.; Patel, H. S. Hydrogen Bonding Properties of Coumarin 151, 500, and 35: The Effect of Substitution at the 7-Amino Position. *J. Phys. Chem. A* **2006**, *110*, 1698−1704.
(48) Azpiroz, J. M.; Infante, I.; Lopez, X.; Ugalde, J. M.; De Angelis, F. A First-Principles Study of II-VI (II = Zn; VI = O, S, Se, Te) Semiconductor Nanostructures. *J. Mater. Chem.* **2012**, *22*, 21453−21465.
(49) Wang, X.; Wang, B.; Tang, L.; Sai, L.; Zhao, J. What Is Atomic Structures of $(ZnO)_{34}$ Magic Cluster? *Phys. Lett. A* **2010**, *374*, 850−853.
(50) Caddeo, C.; Malloci, G.; De Angelis, F.; Colombo, L.; Mattoni, A. Optoelectronic Properties of $(Zno)_{60}$ Isomers. *Phys. Chem. Chem. Phys.* **2012**, *14*, 14293−14298.
(51) Wang, B.; Wang, X.; Zhao, J. Atomic Structure of the Magic $(ZnO)_{60}$ Cluster: First-Principles Prediction of a Sodalite Motif for ZnO Nanoclusters. *J. Phys. Chem. C* **2010**, *114*, 5741−5744.
(52) Badaeva, E.; Feng, Y.; Gamelin, D. R.; Li, X. Investigation of Pure and Co^{2+}-Doped Zno Quantum Dot Electronic Structures Using the Density Functional Theory: Choosing the Right Functional. *New J. Phys.* **2008**, *10*, 055013.
(53) Oprea, C. I.; Panait, P.; Cimpoesu, F.; Ferbinteanu, M.; Girtu, M. A. Density Functional Theory (Dft) Study of Coumarin-Based Dyes Adsorbed on TiO_2 Nanoclusters - Applications to Dye-Sensitized Solar Cells. *Materials* **2013**, *6*, 2372−2392.
(54) Chakrapani, V.; Pendyala, C.; Kash, K.; Anderson, A. B.; Sunkara, M. K.; Angus, J. C. Electrochemical Pinning of the Fermi Level: Mediation of Photoluminescence from Gallium Nitride and Zinc Oxide. *J. Am. Chem. Soc.* **2008**, *130*, 12944−12952.
(55) Matthews, D.; Infelta, P.; Graetzel, M. Calculation of the Photocurrent-Potential Characteristic for Regenerative, Sensitized Semiconductor Electrodes. *Sol. Energy Mater. Sol. Cells* **1996**, *44*, 119−155.
(56) Anderson, N. A.; Lian, T. Ultrafast Electron Injection from Metal Polypyridyl Complexes to Metal-Oxide Nanocrystalline Thin Films. *Coord. Chem. Rev.* **2004**, *248*, 1231−1246.
(57) Hagberg, D. P.; et al. Molecular Engineering of Organic Sensitizers for Dye-Sensitized Solar Cell Applications. *J. Am. Chem. Soc.* **2008**, *130*, 6259−6266.
(58) Hara, K.; Sato, T.; Katoh, R.; Furube, A.; Ohga, Y.; Shinpo, A.; Suga, S.; Sayama, K.; Sugihara, H.; Arakawa, H. Molecular Design of Coumarin Dyes for Efficient Dye-Sensitized Solar Cells. *J. Phys. Chem. B* **2003**, *107*, 597−606.
(59) Zhang, X.; Zhang, J.-J.; Xia, Y.-Y. Molecular Design of Coumarin Dyes with High Efficiency in Dye-Sensitized Solar Cells. *J. Photochem. Photobiol., A* **2008**, *194*, 167−172.
(60) Sanchez-de-Armas, R.; San Miguel, M. A.; Oviedo, J.; Sanz, J. F. Coumarin Derivatives for Dye Sensitized Solar Cells: A TD-DFT Study. *Phys. Chem. Chem. Phys.* **2012**, *14*, 225−233.
(61) Marcus, R. A. Theory of Electron-Transfer Reactions. VI. Unified Treatment for Homogeneous and Electrode Reactions. *J. Chem. Phys.* **1965**, *43*, 679−701.
(62) Marcus, R. A.; Sutin, N. Electron Transfers in Chemistry and Biology. *Biochim. Biophys. Acta, Rev. Bioenerg.* **1985**, *811*, 265−322.
(63) Caddeo, C.; Malloci, G.; Rignanese, G.-M.; Colombo, L.; Mattoni, A. Electronic Properties of Hybrid Zinc Oxide-Oligothiophene Nanostructures. *J. Phys. Chem. C* **2012**, *116*, 8174−8180.
(64) Hagfeldt, A.; Boschloo, G.; Sun, L.; Kloo, L.; Pettersson, H. Dye-Sensitized Solar Cells. *Chem. Rev. (Washington, DC, U. S.)* **2010**, *110*, 6595−6663.
(65) Pastore, M.; De Angelis, F. Computational Modelling of TiO_2 Surfaces Sensitized by Organic Dyes with Different Anchoring Groups: Adsorption Modes, Electronic Structure and Implication for Electron Injection/Recombination. *Phys. Chem. Chem. Phys.* **2012**, *14*, 920−928.
(66) Saba, M. I.; Calzia, V.; Melis, C.; Colombo, L.; Mattoni, A. Atomistic Investigation of the Solid-Liquid Interface between the Crystalline Zinc Oxide Surface and the Liquid Tetrahydrofuran Solvent. *J. Phys. Chem. C* **2012**, *116*, 12644−12648.

DOI: 10.1021/acs.jpca.5b04109
J. Phys. Chem. A XXXX, XXX, XXX−XXX